drones

MDPI

Article

Optimization of Full-Duplex UAV Secure Communication with the Aid of RIS

Huan Lai [1], Dongfen Li [1,*], Fang Xu [1,2], Xiao Wang [1], Jin Ning [1], Yanmei Hu [1] and Bin Duo [1]

[1] College of Computer Science and Cyber Security, Chengdu University of Technology, Chengdu 610059, China
[2] College of Electronic and Information Engineering, Southwest University, Chongqing 400715, China
* Correspondence: lidongfen17@cdut.edu.cn

Abstract: Recently, unmanned aerial vehicles (UAVs) have gained significant popularity and have been extensively utilized in wireless communications. Due to the susceptibility of wireless channels to eavesdropping, interference and other security attacks, UAV communication security faces serious challenges. Therefore, novel solutions need to be investigated for handling corresponding issues. Note that the UAV with full-duplex (FD) mode can actively improve spectral efficiency, and reconfigurable intelligent surface (RIS) can enable the intelligent control of signal reflection for improving transmission quality. Accordingly, the security of UAV communications may be considerably improved by combining the two techniques mentioned above. In this paper, we investigate the performance of secure communication in urban areas, assisted by a FD UAV and an RIS, where the UAV receives sensitive information from the ground users and sends jamming signals to the ground eavesdroppers. Particularly, we propose an approach to jointly optimize the user scheduling, user transmit power, UAV jamming power, RIS phase shift, and UAV trajectory for maximizing the worst-case secrecy rate. However, the non-convexity of the problem makes it difficult to solve. Combining alternating optimization (AO), slack variable techniques, successive convex approximation (SCA), and semi-definite relaxation (SDR), we propose an effective algorithm to obtain a suboptimal solution. According to the simulation results, in contrast to other benchmark schemes, we show that our proposed algorithm can significantly improve the overall secrecy rate.

Keywords: reconfigurable intelligent surface; full duplex; UAV secure communication; power control; UAV trajectory design

Citation: Lai, H.; Li, D.; Xu, F.; Wang, X.; Ning, J.; Hu, Y.; Duo, B. Optimization of Full-Duplex UAV Secure Communication with the Aid of RIS. *Drones* **2023**, *7*, 591. https://doi.org/10.3390/drones7090591

Academic Editors: Panagiotis Sarigiannidis, Abderrahmane Lakas and Mauro Tropea

Received: 15 July 2023
Revised: 8 September 2023
Accepted: 18 September 2023
Published: 20 September 2023

1. Introduction

In recent years, owing to their characteristics of an adaptive altitude, flexibility, and mobility, unmanned aerial vehicles (UAVs) have been extensively applied in diverse areas [1–3]. UAVs already show many advantages in terms of improving the performance of wireless communications in many application scenarios [4,5]. Generally, UAVs can be used as airborne base stations (BSs) to improve the energy efficiency, dependability, capacity, and coverage of wireless networks. However, as the wireless channel is usually shared by many users, UAV-assisted wireless communications face very high eavesdropping risk [6,7].

Over the past decades, communication security mainly depended on the cryptographic encryption techniques deployed at higher protocol stack layers. However, these techniques cause high management costs and heavy computation [8]. The advent of physical layer security (PLS) techniques has significantly enhanced this landscape. It effectively supplements the cryptographic techniques, as its ability does not rely on the computing capabilities of communication devices [9]. As a result, a lot of research has been performed recently to guarantee the secure transmission of UAVs through combining the PLS techniques [10–14]. In order to avoid eavesdropping, UAVs play multiple roles, such as airborne BSs, legitimate receivers, and relays. These roles are strategically supported by the implementation of the

PLS techniques, including beamforming, power allocation, trajectory planning, and so on. Furthermore, UAVs can also serve as friendly jammers to collaboratively transmit jamming signals for interfering with the wiretap channels. This collaborative jamming approach can significantly enhance the security of UAV communication systems. Specifically, in [10], UAVs were used to send artificial interference to the eavesdropper to confuse its reception, which can significantly improve security performance in some cases. In [11], the UAV was used as a mobile BS to jointly optimize the UAV trajectory and power allocation to maximize the average secrecy rate. When the UAV eavesdroppers were dispersed at random in [13], a UAV jammer aided in increasing the secrecy rate. Two UAVs were taken into account in [12], where one UAV transmitted sensitive data to a ground node (GN), and the other one jammed communication by broadcasting noise. Although the security of the UAV communication can be improved with the help of PLS technology, these technologies are not sufficient to address all security issues. Due to the complexity and dynamic nature of UAV communication systems, it is imperative to investigate innovative and efficient technologies to guarantee the security of the UAV communication.

Noticeably, due to its energy-saving, low-cost, simple-to-deploy, and programmable features, RIS is recognized as a disruptive technology in the future 6G communications [15–18]. RIS possesses the capability to passively reflect the incident signals and reconfigure the wireless propagation environment to reduce interference or improve the quality of desired signals [19]. Additionally, RIS has the advantage of low cost and energy consumption, as it operates within a short distance and does not require radio frequency (RF) chains [20]. Consequently, there have been numerous works using RIS in UAV networks to improve their security [14,21–23]. In particular, researchers in [21] jointly optimized the UAV trajectory, power control, and the RIS phase shifter to maximize the secrecy rate. Ref. [22] confirmed that the benefits of RIS in improving UAV communication security can be extended to multi-user scenarios. Furthermore, in [23], the authors considered a multi-antenna UAV and further used RIS to ameliorate the propagation environment, where the secrecy rate was significantly increased. Moreover, due to the line-of-sight (LoS) characteristic of UAVs, aerial malicious UAV eavesdroppers are more likely to establish LoS links with ground BS as compared to ground eavesdroppers, who pose a greater threat in terms of communication security [24]. To better address the threat issue of aerial eavesdropping, the authors in [14] introduced RIS into the system and demonstrated a significant enhancement for communication security. In the aforementioned work, it was shown that by optimizing the distribution and gain of the reflected signals, RIS can enhance the PLS of the UAV communication. In addition, RIS can also significantly reduce the transmit power consumption [25]. Indeed, except for improving the energy efficiency and security, achieving high spectral efficiency is also a key challenge in UAV communications. Enabling UAVs to operate in FD mode may be a promising solution to address such a problem.

Generally, FD technology has been extensively adopted in wireless communication due to its capability of effectively improving spectral efficiency [26–28]. Thus, the extension of FD capabilities to the UAVs emerges as a promising approach to enhance UAV communication security. Specifically, the optimization algorithm proposed in [26], which is used to handle the FD operation, resulted in significant improvement in energy efficiency and secrecy rate. The authors in [27] demonstrated that the FD technology can improve the security performance of wireless communications due to its capability to double the spectrum efficiency. In terms of secrecy performance, the authors in [28] showed that FD systems can outperform half-duplex systems. Note that, in FD mode, the residual self-interference (RSI) is a non-negligible factor that is referred to the interference that occurs when the transmitted signal leaks or reflects back into the receiver's own receiver chain. RSI has detrimental effects on the received signal quality and overall communication performance [29].

Despite lots of studies on secure UAV communications, there are still some limitations that have not been well considered:

(i) Although studies [14,21–23] affirmed a notable enhancement in the security of UAV communication with the aid of RIS, the persistent threat of eavesdropping remains. To address this, additional measures can be implemented to actively diminish the eavesdroppers' capabilities of eavesdropping and further mitigate the risk of information leakage.

(ii) Although studies [27,28] showed that the FD UAVs can enhance communication security, they did not consider the important impact of RSI. Investigating the integration of RIS in an FD UAV system is crucial to determine whether it can address or improve the issues caused by RSI.

(iii) Although the authors in [26] discussed the impact of RSI, it is based on a simplified LoS channel model, which cannot accurately characterize actual environments. In practical urban areas, there may be deviations and losses in security performance that need to be considered.

Motivated by the aforementioned issues, we intend to focus on investigating an RIS-assisted FD UAV secure communication system in urban areas. To facilitate communication between each user and the UAV, the RIS is set up on the building's outside. The UAV operates in FD mode to simultaneously collect private information from the ground users and deliver jamming signals to prevent eavesdropping. Considering the fairness, the worst-case minimal average secrecy rate is maximized by jointly optimizing the user scheduling, user transmit power, UAV jamming power, RIS phase shift, and UAV trajectory. However, the expected secrecy rate function is quite complex, which makes the formulated problem non-convex. Consequently, directly applying existing optimization techniques makes attaining a globally optimal solution difficult. To overcome these difficulties, we begin by deriving a lower bound for the secrecy rate function. Then, the alternating optimization (AO) method provides an efficient iterative algorithm. In particular, we segment the primary problem into five distinct blocks. However, it is important to note that these subproblems remain non-convex. To address this challenge, we introduce slack variables and leverage the successive convex approximation (SCA) and semi0definite relaxation (SDR) techniques to resolve them aptly. Note that our proposed system adopts distinct channel models for different communication links, ensuring a more realistic alignment between the communication effectiveness and actual communication scenarios. According to the simulation results, in contrast to other benchmark schemes, it is shown that our proposed algorithm can significantly improve the overall secrecy rate. Furthermore, compared to the no RIS scheme, the proposed scheme under the adverse influence of RSI has the higher capability to weaken the eavesdropper's ability to eavesdrop.

The paper is organized as follows: In Section 2, we present the problem formulation and system model. Section 3 outlines the methodology used to address the formulated problem. In Section 4, we present the numerical results and provide a comprehensive discussion. Finally, Section 5 concludes the paper. The key notations are outlined in Table 1.

Table 1. List of major notations.

Notation	Description
M	The number of ground users
N	The number of RIS reflecting elements
$\mathbf{s}_G$	Horizontal location of ground users
$\mathbf{s}_E$	Horizontal location of the Eve
$\mathbf{s}_R$	Horizontal location of the RIS
z_R	RIS placement height
$\mathbf{t}_0, \mathbf{t}_F$	UAV initial and final horizontal locations
z_U	UAV flight altitude
$V_{\max}$	Maximum speed of UAV
Ψ	Highest UAV horizontal flight distance within each time slot
T, Ω	The length of flight period, the number of time slots
δ_t	Each time slot's duration

Table 1. *Cont.*

Notation	Description
$\tilde{h}_1, \tilde{h}_2, \tilde{h}_3$	The random scattering component
λ	The carrier wavelength
d	The distance of antenna separation
$\overline{P_G}, P_G^{\max}$	Ground user average and peak transmit power
$\overline{P_U}, P_U^{\max}$	UAV's average and peak jamming power
$\kappa_D, \kappa_R, \kappa_L$	Corresponding path loss exponent
$\varrho_{G,R}, \varrho_{R,E}$	The Rician factor of the G-R, R-E link
ρ	The path loss at the reference distance
$\digamma$	Exponential distribution with unit mean accounting
σ^2	The additive white Gaussian noise power
σ^2_{RSI}	The average loop interference level
$\mathbf{\Theta}$	RIS diagonal phase shift matrix
θ_n	The n-th reflecting element's phase shift
β_i	The binary variable of indicating whether user i is served by the UAV
$(\hat{\cdot}), (\check{\cdot})$	Maximum value, Minimum value

2. System Model and Problem Formulation

In this paper, we focus on a UAV-enabled wireless communication system as depicted in Figure 1. The system consists of a group of ground users transmitting confidential information to a UAV. The UAV flies from the starting point to the terminal point at a fixed altitude for a specified duration of time T. At the same time, a ground eavesdropper (denoted by Eve) attempts to intercept the communication. To safeguard the data transmission, an RIS is deployed on the building's outside to reflect incident signals from each user and the UAV effectively. The RIS consists of $N = N_x \times N_z$ reflecting elements, with a uniform rectangular array (URA) of size $N_x \times N_z$. The horizontal coordinate and height of the RIS elements are represented by $\mathbf{s}_R = [x_R, y_R]^T$ and z_R, respectively. The set of the ground users is represented as $\mathcal{M}$, where $|\mathcal{M}| = M$, and the i-th ground user's horizontal coordinate is represented as $\mathbf{s}_G = [x_i, y_i]^T \in R^{2\times 1}, i \in \mathcal{M}$. The ground Eve is positioned with a horizontal coordinate $\mathbf{s}_E = [x_E, y_E]^T$. We assume that the UAV operates in FD mode to simultaneously broadcast jamming signals to interfere with the Eve and receive sensitive information. The Eve and each ground user are equipped with receive and transmit antennas, respectively. As a result, in this system, all communication links are composed of direct and reflective links.

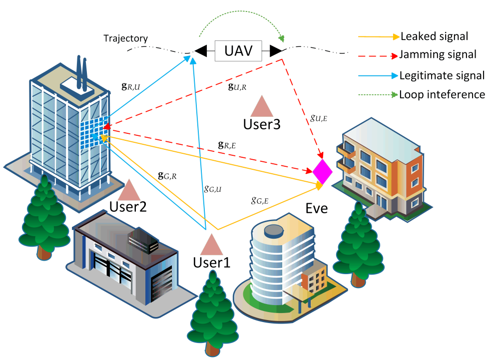

Figure 1. RIS-aided full-duplex UAV secure communication.

2.1. UAV Trajectory Model

As we know, UAV trajectory designing is one of the means to enhance the performance of UAV communication at the PLS. UAV trajectories can be designed through sensible path planning, enabling optimal communication and interference strategies within specific areas. In this system, the ground users are assumed to be served by the UAV, and the total duration T is partitioned into Ω equal time slots. Consequently, we have $T = \delta_t\Omega$, where δ_t

represents each time slot's duration and needs to be set as the optimal value. During the flight duration, the UAV flies from the starting point to the terminal at a constant altitude specified as z_U. The horizontal trajectory can be roughly described by a series of points denoted by $\mathbf{t} = \{\mathbf{t}[\omega] \triangleq [x[\omega], y[\omega]]^T\}, \omega \in \{0, \ldots, \Omega\}$. The UAV trajectory has to be subject to the following restrictions:

$$\mathbf{t}[0] = \mathbf{t}_0, \mathbf{t}[\Omega] = \mathbf{t}_F, \tag{1}$$

where $\mathbf{t}_0 = [x_0, y_0]^T$ is the UAV starting horizontal coordinate and $\mathbf{t}_\mathrm{F} = [x_F, y_F]^T$ is the UAV final horizontal coordinate. Given a maximum UAV speed of $V_{\max}$ in meter/second (m/s), within each time slot, the farthest horizontal distance that the UAV can fly is $\Psi = V_{\max}\delta_\mathrm{t}$, which satisfies

$$||\mathbf{t}[\omega+1] - \mathbf{t}[\omega]||^2 \leq \Psi^2, \omega = 0, \ldots, \Omega - 1. \tag{2}$$

2.2. Direct Channel Model

The direct links are the link from the ground users to the UAV (G-U link), the link from the UAV to the Eve (U-E link), and the link from the ground users to the Eve (G-E link), respectively. Following [26], we assume that all channels follow the Rayleigh fading channel model, as the communication is easily blocked by the obstructions in an urban environment.

For the G-U link, the U-E link, and the G-E link, the channel gain can be denoted as $g_{G,U}[\omega] \in \mathbb{C}$, $g_{U,E}[\omega] \in \mathbb{C}$ and $g_{G,E} \in \mathbb{C}$, respectively, given by

$$g_{G,U}[\omega] = \sqrt{\rho \times dist_{G,U}[\omega]^{-\kappa_D}}\, \tilde{h}_1, \tag{3}$$

$$g_{U,E}[\omega] = \sqrt{\rho \times dist_{U,E}[\omega]^{-\kappa_D}}\, \tilde{h}_2, \tag{4}$$

$$g_{G,E} = \sqrt{\rho \times dist_{G,E}{}^{-\kappa_D}}\, \tilde{h}_3, \tag{5}$$

where ρ is the reference distance D_0's path loss for D_0 = 1 m; κ_D is the corresponding path loss exponent; $\tilde{h}_1, \tilde{h}_2$ and $\tilde{h}_3 \sim \mathcal{CN}(0,1)$ represent the random scattering component; and $dist_{G,U}[\omega] = \sqrt{z_U^2 + ||\mathbf{s}_G - \mathbf{t}[\omega]||^2}$, $dist_{U,E}[\omega] = \sqrt{z_U^2 + ||\mathbf{t}[\omega] - \mathbf{s}_E||^2}$, and $dist_{G,E} = \sqrt{||\mathbf{s}_G - \mathbf{s}_E||^2}$ denote the distances of the G-U link, the U-E link, and the G-E link.

2.3. Reflecting Channel Model

The reflecting links are the U-R link (from the UAV to the RIS), the R-U link (from the UAV to the ground users), the G-R link (from the ground users to the RIS), and the R-E link (from the RIS to the Eve). The LoS channel [30] is assumed to be used by the U-R and the R-U links. Therefore, $\mathbf{g}_{R,U}[\omega] \in \mathbb{C}^{N\times 1}$ may be used to represent the channel model of the R-U link, which is given by

$$\mathbf{g}_{R,U}[\omega] = \sqrt{\rho \times dist_{R,U}^{-\kappa_L}[\omega]}\, \mathbf{g}_{R,U}^{\mathrm{LOS}}[\omega], \tag{6}$$

where κ_L is the corresponding path loss exponent, $dist_{R,U}[\omega] = \sqrt{||\mathbf{s}_R - \mathbf{t}[\omega]||^2 + z_R^2}$ represents the distance of the R-U link during the ω-th time slot, and $\mathbf{g}_{R,U}^{\mathrm{LOS}}[\omega]$ can be denoted as

$$\mathbf{g}_{R,U}^{\mathrm{LOS}}[\omega] = \boldsymbol{\varpi}_y^{R,U}[\omega] \otimes \boldsymbol{\varpi}_x^{R,U}[\omega], \tag{7}$$

where

$$\boldsymbol{\varpi}_x^{R,U}[\omega] = \left[1, e^{-j\frac{2\pi}{\lambda}d\cos\phi_{R,U}[\omega]\sin\varphi_{R,U}[\omega]}, \ldots, e^{-j\frac{2\pi}{\lambda}(M_x-1)d\cos\phi_{R,U}[\omega]\sin\varphi_{R,U}[\omega]}\right]^T,$$

$$\boldsymbol{\varpi}_y^{R,U}[\omega] = \left[1, e^{-j\frac{2\pi}{\lambda}d\sin\phi_{R,U}[\omega]\sin\varphi_{R,U}[\omega]}, \ldots, e^{-j\frac{2\pi}{\lambda}(M_z-1)d\sin\phi_{R,U}[\omega]\sin\varphi_{R,U}[\omega]}\right]^T,$$

$\cos\phi_{R,U}[\omega]\sin\varphi_{R,U}[\omega] = \frac{x_R - x[\omega]}{dist_{R,U}[\omega]}$, $\sin\phi_{R,U}[\omega]\sin\varphi_{R,U}[\omega] = \frac{z_R}{dist_{R,U}[\omega]}$, $\phi_{R,U}[\omega]$ and $\varphi_{R,U}[\omega]$ represent the LoS component's azimuth and elevation angles within the ω-th time slot, λ is the carrier wavelength, and d is the distance of antenna separation. A similar process may be employed for constructing the channel model from the UAV to the RIS (U-R) link and can be denoted as $\mathbf{g}_{U,R}[\omega] \in \mathbb{C}^{N\times 1}$.

Following [31], we assume that the link between the ground user and the RIS (G-R link) and the link between the RIS and the Eve (R-E link) are Rician fading channel models. Therefore, the channel model of the G-R link can be denoted as $\mathbf{g}_{G,R} \in \mathbb{C}^{N\times 1}$, given by

$$\mathbf{g}_{G,R} = \sqrt{\rho \times dist_{G,R}^{-\kappa_R}}\left(\sqrt{\frac{1}{\varrho_{G,R}+1}}\mathbf{g}_{G,R}^{\mathrm{NLOS}} + \sqrt{\frac{\varrho_{G,R}}{\varrho_{G,R}+1}}\mathbf{g}_{G,R}^{\mathrm{LOS}}\right), \tag{8}$$

where κ_R is the corresponding path loss exponent, $dist_{G,R} = \sqrt{z_R^2 + ||\mathbf{s}_G - \mathbf{s}_R||^2}$ denotes the distance of the G-R link within the time slot ω, $\varrho_{G,R}$ is the G-R link's Rician factor, $\mathbf{g}_{G,R}^{\mathrm{LOS}}$ represents the deterministic LoS component, and $\mathbf{g}_{G,R}^{\mathrm{NLOS}}$ is the non-LoS (NLoS) component following a circularly symmetric complex Gaussian (CSCG) distribution with zero mean and unit variance. Specifically, $\mathbf{g}_{G,R}^{\mathrm{LOS}}$ is dependent on the trajectory of the UAV, and is denoted by

$$\mathbf{g}_{G,R}^{\mathrm{LOS}} = \boldsymbol{\varpi}_y^{G,R} \otimes \boldsymbol{\varpi}_x^{G,R}, \tag{9}$$

where

$$\begin{aligned}\boldsymbol{\varpi}_x^{G,R} &= \left[1, e^{-j\frac{2\pi}{\lambda}d\cos\phi_{G,R}\sin\varphi_{G,R}}, \ldots, e^{-j\frac{2\pi}{\lambda}(M_x-1)d\cos\phi_{G,R}\sin\varphi_{G,R}}\right]^T,\\ \boldsymbol{\varpi}_y^{G,R} &= \left[1, e^{-j\frac{2\pi}{\lambda}d\sin\phi_{G,R}\sin\varphi_{G,R}}, \ldots, e^{-j\frac{2\pi}{\lambda}(M_z-1)d\sin\phi_{G,R}\sin\varphi_{G,R}}\right]^T.\end{aligned}$$

$\cos\phi_{G,R}\sin\varphi_{G,R} = \frac{x_R - x_i}{dist_{G,R}}$, $\sin\phi_{G,R}\sin\varphi_{G,R} = \frac{z_R}{dist_{G,R}}$, $\phi_{G,R}$ and $\varphi_{G,R}$ denote the LoS component's azimuth and elevation angles, respectively.

A similar analysis process can be applied to the R-E link. The corresponding channel power gain can be represented as $\mathbf{g}_{R,E} \in \mathbb{C}^{N\times 1}$ and given by

$$\mathbf{g}_{R,E} = \sqrt{\rho \times dist_{R,E}^{-\kappa_R}}\left(\sqrt{\frac{1}{\varrho_{R,E}+1}}\mathbf{g}_{R,E}^{\mathrm{NLOS}} + \sqrt{\frac{\varrho_{R,E}}{\varrho_{R,E}+1}}\mathbf{g}_{R,E}^{\mathrm{LOS}}\right), \tag{10}$$

where $dist_{R,E} = \sqrt{z_R^2 + ||\mathbf{s}_R - \mathbf{s}_E||^2}$ denotes the distance of the R-E link within the time slot ω, and $\varrho_{R,E}$ is the R-E link's Rician factor. The CSCG distribution with a zero mean and a unit variance is applicable for both NLoS components $\mathbf{g}_{R,E}^{\mathrm{NLOS}}$. Specifically, $\mathbf{g}_{R,E}^{\mathrm{LOS}}$ is dependent on the trajectory of the UAV, and is denoted by

$$\mathbf{g}_{R,E}^{\mathrm{LOS}} = \boldsymbol{\varpi}_y^{R,E} \otimes \boldsymbol{\varpi}_x^{R,E}, \tag{11}$$

where

$$\begin{aligned}\boldsymbol{\varpi}_x^{R,E} &= \left[1, e^{-j\frac{2\pi}{\lambda}d\cos\phi_{R,E}\sin\varphi_{R,E}}, \ldots, e^{-j\frac{2\pi}{\lambda}(M_x-1)d\cos\phi_{R,E}\sin\varphi_{R,E}}\right]^T,\\ \boldsymbol{\varpi}_y^{R,E} &= \left[1, e^{-j\frac{2\pi}{\lambda}d\sin\phi_{R,E}\sin\varphi_{R,E}}, \ldots, e^{-j\frac{2\pi}{\lambda}(M_z-1)d\sin\phi_{R,E}\sin\varphi_{R,E}}\right]^T.\end{aligned}$$

Here, $\cos\phi_{R,E}\sin\varphi_{R,E} = \frac{x_R - x_E}{dist_{R,E}}$ and $\sin\phi_{R,E}\sin\varphi_{R,E} = \frac{z_R}{dist_{R,E}}$.

2.4. Secrecy Rate

In the ω-th time slot, the channel gain of the direct links and the reflecting links from the ground user and the Eve to the UAV through RIS can be denoted by

$$y_U[\omega] = g_{G,U}[\omega] + \mathbf{g}_{R,U}^H[\omega]\mathbf{\Theta}[\omega]\mathbf{g}_{G,R}, \tag{12}$$
$$y_{E1}[\omega] = g_{G,E} + \mathbf{g}_{R,E}^H\mathbf{\Theta}[\omega]\mathbf{g}_{G,R}, \tag{13}$$
$$y_{E2}[\omega] = g_{U,E}[\omega] + \mathbf{g}_{R,E}^H\mathbf{\Theta}[\omega]\mathbf{g}_{U,R}[\omega], \tag{14}$$

where $\mathbf{\Theta}[\omega] = \mathrm{diag}(e^{j\theta_1[\omega]}, \ldots, e^{j\theta_N[\omega]})$ is the RIS diagonal phase shift matrix, $\theta_n[\omega] \in [0, 2\pi)$, $n \in \mathcal{N} = \{1, \ldots, N\}$ is the n-th reflecting element's phase shift and $\mathrm{diag}(\mathbf{x})$ is the diagonal matrix.

The residual self-interference (RSI) at the UAV, which is challenging to be completely eliminated in practical FD mode, has a great impact on the secure performance of communication. In this case, we define h_{JJ} as the channel gain caused by the RSI. It represents the incomplete loop interference cancellation from the UAV broadcasting antenna to its receiving antenna. Rayleigh fading is a typical model for the RSI channel h_{JJ} derived independently from $\mathcal{CN}(0, \sigma_{RSI}^2)$, where the average loop interference with $\mathbb{E}[|h_{JJ}|^2] = \sigma_{RSI}^2$ is defined as σ_{RSI}^2.

Let $P_G[\omega]$ represent the transmit power for ground users, and $P_U[\omega]$ denote the UAV jamming power within the ω-th time slot, respectively. The average and peak power restrictions are shown below:

$$\overline{P_j} = \frac{1}{\Omega}\sum_{\omega=1}^{\Omega} P_j[\omega], 0 \le P_j[\omega] \le P_j^{\max}, j \in G, U \tag{15}$$

where $\overline{P_j} \le P_j^{\max}$. Then, within the time slot ω, the constraints for the achievable rates of the UAV and the Eve in bits/second/Hertz (bps/Hz) are given by

$$\begin{aligned} R_U[\omega] &= \mathbb{E}_1\left[\log_2\left(1 + \frac{P_G[\omega]|y_U[\omega]|^2}{\sigma^2 + P_U[\omega]|h_{JJ}|^2}\right)\right] \\ &\overset{(a)}{\ge} \log_2\left(1 + \frac{P_G[\omega]|y_U[\omega]|^2}{\sigma^2 + P_U[\omega]\sigma_{RSI}^2}\right) \triangleq \check{R}_U[\omega], \end{aligned} \tag{16}$$

$$\begin{aligned} R_E[\omega] &= \mathbb{E}_2\left[\log_2\left(1 + \frac{P_G[\omega]|y_{E1}[\omega]|^2}{\sigma^2 + P_U[\omega]|y_{E2}[\omega]|^2}\digamma\right)\right] \\ &\overset{(b)}{\le} \log_2\left(1 + \frac{P_G[\omega]|y_{E1}[\omega]|^2}{\sigma^2 + P_U[\omega]|y_{E2}[\omega]|^2}\right) \triangleq \hat{R}_E[\omega], \end{aligned} \tag{17}$$

where $\digamma$ follows an exponential distribution with unit mean accounting, σ^2 represents the power of additive white Gaussian noise at the respective receiver, and $\mathbb{E}_1\{\cdot\}$ and $\mathbb{E}_2\{\cdot\}$ denote the expectation operators with respect to $|h_{JJ}|^2$ and $\digamma$. With regard to the variables, $\log_2\left(1 + \frac{P_G[\omega]|y_U[\omega]|^2}{\sigma^2 + P_U[\omega]|h_{JJ}|^2}\right)$ and $\log_2\left(1 + \frac{P_G[\omega]|y_{E1}[\omega]|^2}{\sigma^2 + P_U[\omega]|y_{E2}[\omega]|^2}\digamma\right)$ are convex (concave). With Jensen's inequality, we can show that (a) in (16) and (b) in (17) hold.

At each time slot, there is only one scheduled user communicating with the UAV under time division multiple access (TDMA). The binary variable $\beta_i[\omega]$ is introduced to indicate whether user i is served by the UAV within the ω-th time slot. If $\beta_i[\omega] = 1$, it implies that user i is served; otherwise, if $\beta_i[\omega] = 0$. These constraints can be formulated as given below:

$$\sum_{i=1}^{M} \beta_i[\omega] \le 1, \forall \omega, \tag{18}$$
$$\beta_i[\omega] \in \{0, 1\}, \forall i, \omega. \tag{19}$$

As a result, within each time slot, the achievable average secrecy rate is denoted by

$$R_{\text{sec}}[\omega] = \left[\frac{1}{\Omega} \sum_{\omega=1}^{\Omega} \beta_i[\omega] (\check{R}_U[\omega] - \hat{R}_E[\omega]) \right]^+, \tag{20}$$

where $[x]^+ = \max(x, 0)$. By setting $P_G[\omega] = 0, \forall \omega$, it should be noted that the operator $[\cdot]^+$ may be omitted since the actual value of (20) is always non-negative.

2.5. Problem Formulation

In this study, by jointly optimizing the user scheduling $\mathbf{A} = \{\beta_i[\omega], \forall i\}_{\omega=1}^{\Omega}$, the user transmit power $\mathbf{P}_G \triangleq \{P_G[\omega]\}_{\omega=1}^{\Omega}$, the UAV jamming power $\mathbf{P}_U \triangleq \{P_U[\omega]\}_{\omega=1}^{\Omega}$, the RIS phase shift $\boldsymbol{\Theta} \triangleq \{\boldsymbol{\Theta}[\omega]\}_{\omega=1}^{\Omega}$ and the horizontal UAV trajectory $\boldsymbol{\mathcal{T}} \triangleq \{\mathbf{t}[\omega]\}_{\omega=1}^{\Omega}$ over the flight time duration of T, we aim to maximize the worst-case achievable average secrecy rate of the UAV for each user. Consequently, the problem can be described as

$$\max_{\mathbf{A}, \mathbf{P}_G, \mathbf{P}_U, \boldsymbol{\Theta}, \boldsymbol{\mathcal{T}}, \zeta} \ \zeta \tag{21}$$

$$\text{s.t.} \ R_{\text{sec}}[\omega] \geq \zeta, \tag{22}$$

$$(1) - (2), (15), (18), (19).$$

Although the constraints in (1), (2) and (15) are convex, solving problem (21) optimally is still challenging. The reasons are shown as follows. First of all, with respect to $\mathbf{A}, \mathbf{P}_G, \mathbf{P}_U, \boldsymbol{\Theta}$ and $\boldsymbol{\mathcal{T}}$, constraint (22) is not jointly convex. Second, due to the binary variable constraints (18) and (19), solving the mixed-integer optimization problem is difficult. As a result, to achieve a suboptimal solution for such an optimization problem, we present an efficient algorithm in Section 3.

3. Proposed Algorithm

In this section, we focus on solving the joint optimization problem mentioned above. However, due to the coupled optimization variables $\mathbf{A}$, $\mathbf{P}_G$, $\mathbf{P}_U$, $\boldsymbol{\Theta}$ and $\boldsymbol{\mathcal{T}}$ in the objective function, solving problem (21) is quite challenging. We propose an efficient algorithm to deal with this issue. To be more precise, we decompose problem (21) into five subproblems.

3.1. Optimization of User Scheduling

The user scheduling problem can be optimized with the given ground user transmit power $\mathbf{P}_G$, the UAV jamming power $\mathbf{P}_U$, the RIS phase shift matrix $\boldsymbol{\Theta}$, and the UAV trajectory $\boldsymbol{\mathcal{T}}$. We relax (19) into continuous variables to make the problem tractable. The problem can be specified by

$$\max_{\mathbf{A}, \zeta} \ \zeta \tag{23}$$

$$\text{s.t.} \ R_{sec}[\omega] \geq \zeta, \tag{24}$$

$$0 \leq \beta_i[\omega] \leq 1, \tag{25}$$

$$(18).$$

As a result, problem (23) can be effectively addressed using CVX because it is a standard linear programming problem. We can find the optimal solution to problem (23) and subsequently obtain the integer solution using the rounding method.

3.2. Optimization of the User Transmit Power

The optimization subproblem of the ground user transmit power $\mathbf{P}_G$ with given $\mathbf{A}$, $\mathbf{P}_U$, $\boldsymbol{\Theta}$, and $\boldsymbol{\mathcal{T}}$, reduces to

$$\max_{\mathbf{P}_G,\zeta} \ \zeta \tag{26}$$

$$\text{s.t.} \ \frac{1}{\Omega}\sum_{\omega=1}^{\Omega}\beta_i[\omega][\log_2(1+\chi_i[\omega]P_G[\omega]) - \log_2(1+\psi_i[\omega]P_G[\omega])] \geq \zeta, \tag{27}$$

$$(15),$$

where $\chi_i[\omega] = \frac{|g_{G,U}[\omega]+\mathbf{g}_{R,U}^H[\omega]\mathbf{\Theta}[\omega]\mathbf{g}_{G,R}|^2}{\sigma^2+P_U[\omega]\sigma_{RSI}^2}$, $\psi_i[\omega] = \frac{|g_{G,E}+\mathbf{g}_{R,E}^H\mathbf{\Theta}[\omega]\mathbf{g}_{G,R}|^2}{\sigma^2+P_U[\omega]|g_{U,E}[\omega]+\mathbf{g}_{R,E}^H\mathbf{\Theta}[\omega]\mathbf{g}_{U,R}[\omega]|^2}$. Based on previous work [32], the optimal solution can be obtained as follows:

$$P_G^{op}[\omega] = \begin{cases} \min([\tilde{P}[\omega]]^+, P_G^{\max}) & \chi_i[\omega] > \psi_i[\omega] \\ 0 & \chi_i[\omega] \leq \psi_i[\omega] \end{cases}, \tag{28}$$

where

$$\tilde{P}[\omega] = \sqrt{(\frac{1}{2\psi_i[\omega]} - \frac{1}{2\chi_i[\omega]})^2 + \frac{1}{\eta \ln 2}(\frac{1}{\psi_i[\omega]} - \frac{1}{\chi_i[\omega]})} - \frac{1}{2\psi_i[\omega]} - \frac{1}{2\chi_i[\omega]}. \tag{29}$$

Note that one-dimensional bisection search may be used to obtain $\eta \geq 0$ in (29), which guarantees that the constraints in (15) are satisfied as long as $P_i^{op}[\omega]$ is attained.

3.3. Optimization of the UAV Jamming Power

The UAV jamming power $\mathbf{P}_U$ Optimization Problem with given $\mathbf{A}$, $\mathbf{P}_G$, $\mathbf{\Theta}$ and $\mathcal{T}$ may be described as follows:

$$\max_{\mathbf{P}_U,\zeta} \ \zeta \tag{30}$$

$$\begin{aligned} \text{s.t.} \ \frac{1}{\Omega}\sum_{\omega=1}^{\Omega}\beta_i[\omega][&\log_2(P_U[\omega]\alpha_0+1+F_\omega) - \log_2(P_U[\omega]\alpha_0+1) \\ &- \log_2(W_\omega P_U[\omega]+1+d_\omega) + \log_2(W_\omega P_U[\omega]+1)] \geq \zeta, \end{aligned} \tag{31}$$

$$(15),$$

where $\alpha_0 = \frac{\sigma_{RSI}^2}{\sigma^2}$, $d_\omega = \frac{P_G[\omega]|g_{G,E}+\mathbf{g}_{R,E}^H\mathbf{\Theta}[\omega]\mathbf{g}_{G,R}|^2}{\sigma^2}$, $F_\omega = \frac{P_G[\omega]|g_{G,U}[\omega]+\mathbf{g}_{R,U}^H[\omega]\mathbf{\Theta}[\omega]\mathbf{g}_{G,R}|^2}{\sigma^2}$, and $W_\omega = \frac{|g_{U,E}[\omega]+\mathbf{g}_{R,E}^H\mathbf{\Theta}[\omega]\mathbf{g}_{U,R}[\omega]|^2}{\sigma^2}$. To avoid the non-convexity of the optimization issue, the SCA technique is used to approximately transform it to a convex optimization problem by following [33]. Since $\log_2(P_U[\omega]\alpha_0+1)$ and $\log_2(W_\omega P_U[\omega]+1+d_\omega)$ are concave functions with respect to $P_U[\omega]$, the first-order Taylor expansion's local upper bound is around a specific point $P_U^{kk0}[\omega]$ as shown below:

$$\log_2(P_U[\omega]\alpha_0+1) \leq \log_2(P_U^{kk0}[\omega]\alpha_0+1) + \frac{\alpha_0(P_U[\omega]-P_U^{kk0}[\omega])}{\ln 2(P_U^{kk0}[\omega]\alpha_0+1)}, \tag{32}$$

$$\log_2(P_U[\omega]W_\omega+1+d_\omega) \leq \log_2(P_U^{kk0}[\omega]W_\omega+1+d_\omega) + \frac{W_\omega(P_U[\omega]-P_U^{kk0}[\omega])}{\ln 2(P_U^{kk0}[\omega]W_\omega+1+d_\omega)}. \tag{33}$$

By replacing the local upper bounds in (32) and (33) using the terms $\log_2(P_U[\omega]\alpha_0+1)$ and $\log_2(W_\omega P_U[\omega]+1+d_\omega)$ in the objective function, problem (30) can be transformed to the following convex optimization problem (34):

$$\max_{\mathbf{P}_U,\zeta} \ \zeta \tag{34}$$

$$\text{s.t.} \ \frac{1}{\Omega}\sum_{\omega=1}^{\Omega}\beta_i[\omega][\log_2(P_U[\omega]\alpha_0+1+F_\omega) + \log_2(W_\omega P_U[\omega]+1)$$

$$-\log_2(P_U[\omega]\alpha_0+1)-\log_2(W_\omega P_U[\omega]+1+d_\omega)$$
$$-\frac{\alpha_0(P_U[\omega]-P_U^{kk0}[\omega])}{\ln 2(P_U^{kk0}[\omega]\alpha_0+1)}-\frac{W_\omega(P_U[\omega]-P_U^{kk0}[\omega])}{\ln 2(P_U^{kk0}[\omega]W_\omega+1+d_\omega)}]\geq\zeta, \tag{35}$$

(15).

Therefore, problem (34) can be effectively addressed using CVX.

3.4. Optimization of the Phase Shift Matrix $\boldsymbol{\Theta}$

Given $\mathbf{A}$, $\mathbf{P}_G$, $\mathbf{P}_U$ and $\boldsymbol{\mathcal{T}}$, with the aid of the slack variable $\boldsymbol{\tau}=\tau[\omega]_{\omega=1}^{\Omega}$, the phase shift matrix $\boldsymbol{\Theta}$ optimization problem is shown as below. Let $\mathbf{q}[\omega]=[q_1[\omega],q_2[\omega],...,q_N[\omega]]^T$, $\left(q_n[\omega]=e^{j\theta_n[\omega]},n\in N,\forall\omega\right)$, $\mathbf{w}[\omega]=[\mathbf{q}^T[\omega],1]^T$, $C_{G,U}[\omega]=\frac{P_G[\omega]|g_{G,U}[\omega]+\mathbf{g}_{R,U}^H[\omega]\boldsymbol{\Theta}[\omega]\mathbf{g}_{G,R}|^2}{\sigma^2+P_U[\omega]\sigma_{RSI}^2}$, $C_{G,E}[\omega]=P_G[\omega]|g_{G,E}+\mathbf{g}_{R,E}^H\boldsymbol{\Theta}[\omega]\mathbf{g}_{G,R}|^2$, and $C_{U,E}[\omega]=P_U[\omega]|g_{U,E}[\omega]+\mathbf{g}_{R,E}^H\boldsymbol{\Theta}[\omega]\mathbf{g}_{U,R}[\omega]|^2$. Thus, the following equalities can hold, shown as follows:

$$C_{G,U}[\omega]=y_W[\omega]+\mathbf{w}^H[\omega]\boldsymbol{\Phi}_W[\omega]\mathbf{w}[\omega], \tag{36}$$
$$C_{G,E}[\omega]=y_I[\omega]+\mathbf{w}^H[\omega]\boldsymbol{\Phi}_I[\omega]\mathbf{w}[\omega], \tag{37}$$
$$C_{U,E}[\omega]=y_U[\omega]+\mathbf{w}^H[\omega]\boldsymbol{\Phi}_U[\omega]\mathbf{w}[\omega], \tag{38}$$

where

$$y_W[\omega]=\frac{P_G[\omega]g_{G,U}^H[\omega]g_{G,U}[\omega]}{\sigma^2+P_U[\omega]\sigma_{RSI}^2}, y_I[\omega]=P_G[\omega]g_{G,E}^Hg_{G,E}, y_U[\omega]=P_U[\omega]g_{U,E}^H[\omega]g_{U,E}[\omega],$$
$$\boldsymbol{\Phi}_W[\omega]=\frac{P_G[\omega]}{\sigma^2+P_U[\omega]\sigma_{RSI}^2}\begin{bmatrix}g_{W1}[\omega] & g_{W2}[\omega]\\ g_{W3}[\omega] & 0\end{bmatrix}, \boldsymbol{\Phi}_U[\omega]=P_U[\omega]\begin{bmatrix}g_{U1}[\omega] & g_{U2}[\omega]\\ g_{U3}[\omega] & 0\end{bmatrix}, \text{and}$$
$$\boldsymbol{\Phi}_I[\omega]=P_G[\omega]\begin{bmatrix}g_{I1}[\omega] & g_{I2}[\omega]\\ g_{I3}[\omega] & 0\end{bmatrix}.$$

Here,

$$g_{W1}[\omega]=\text{diag}(\mathbf{g}_{R,U}^H[\omega]^*)\mathbf{g}_{G,R}^*\mathbf{g}_{G,R}^T\text{diag}(\mathbf{g}_{R,U}^H[\omega]), g_{W2}[\omega]=\text{diag}(\mathbf{g}_{R,U}^H[\omega]^*)\mathbf{g}_{G,R}^*g_{G,U}^T[\omega],$$
$$g_{W3}[\omega]=g_{G,U}^*[\omega]\mathbf{g}_{G,R}^T\text{diag}(\mathbf{g}_{R,U}^H), g_{U1}[\omega]=\text{diag}(\mathbf{g}_{R,E}^{H}{}^*)\mathbf{g}_{U,R}^*[\omega]\mathbf{g}_{U,R}^T[\omega]\text{diag}(\mathbf{g}_{R,E}^H),$$
$$g_{U2}[\omega]=\text{diag}(\mathbf{g}_{R,E}^{H}{}^*)\mathbf{g}_{U,R}^*[\omega]g_{U,E}^T[\omega], g_{U3}[\omega]=g_{U,E}^*[\omega]\mathbf{g}_{U,R}^T[\omega]\text{diag}(\mathbf{g}_{R,E}^H),$$
$$g_{I1}[\omega]=\text{diag}(\mathbf{g}_{R,E}^{H}{}^*)\mathbf{g}_{G,R}^*\mathbf{g}_{G,R}^T\text{diag}(\mathbf{g}_{R,E}^H), g_{I2}[\omega]=\text{diag}(\mathbf{g}_{R,E}^{H}{}^*)\mathbf{g}_{G,R}^*g_{G,E}^T,$$
$$g_{I3}[\omega]=g_{G,E}^*\mathbf{g}_{G,R}^T\text{diag}(\mathbf{g}_{\mathrm{R,E}}^{\mathrm{H}}).$$

Here, the superscript $*$ denotes the conjugate operator. The optimization of the phase shift matrix $\boldsymbol{\Theta}$ is further reduced to

$$\max_{\mathbf{w},\boldsymbol{\tau},\zeta}\ \zeta \tag{39}$$
$$\text{s.t. } \frac{1}{\Omega}\sum_{\omega=1}^{\Omega}\beta_i[\omega][\log_2(1+\mathbf{w}^H[\omega]\boldsymbol{\Phi}_W[\omega]\mathbf{w}[\omega]+y_W[\omega])$$
$$-\log_2(1+\tau[\omega])]\geq\zeta, \tag{40}$$
$$\frac{\mathbf{w}^H[\omega]\boldsymbol{\Phi}_I[\omega]\mathbf{w}[\omega]+y_I[\omega]}{\mathbf{w}^H[\omega]\boldsymbol{\Phi}_U[\omega]\mathbf{w}[\omega]+y_U[\omega]+\sigma^2}\leq\tau[\omega], \tag{41}$$
$$|q_n[\omega]|=1. \tag{42}$$

Since $-\log_2(1+\tau[\omega])$ is not concave with respect to $\tau[\omega]$, finding the optimal solution for problem (39) is challenging. It is known that a convex function's first-order Taylor expansion is its global underestimator and a concave function's global overestimator, respectively. Accordingly, in order to resolve problem (39), we intend to use the SCA approach. The first-order Taylor expansions of $\log_2(1+\tau[\omega])$ at the specified point $\boldsymbol{\tau}_0 = \tau_0[\omega]_{\omega=1}^{\Omega}$ is denoted as follows:

$$\log_2(1+\tau[\omega]) \leq \log_2(1+\tau_0[\omega]) + \frac{(\tau[\omega]-\tau_0[\omega])}{\ln 2(1+\tau_0[\omega])}. \tag{43}$$

Hence, we modify problem (39) to

$$\max_{\mathbf{w},\boldsymbol{\tau},\zeta} \ \zeta \tag{44}$$

$$\text{s.t.} \ \frac{1}{\Omega}\sum_{\omega=1}^{\Omega} \beta_i[\omega][\log_2(1+\mathbf{w}^H[\omega]\boldsymbol{\Phi}_W[\omega]\mathbf{w}[\omega]+y_W[\omega]) - \frac{\tau[\omega]}{\ln 2(1+\tau_0[\omega])}] \geq \zeta, \tag{45}$$

$$\frac{\mathbf{w}^H[\omega]\boldsymbol{\Phi}_I[\omega]\mathbf{w}[\omega]+y_I[\omega]}{\mathbf{w}^H[\omega]\boldsymbol{\Phi}_U[\omega]\mathbf{w}[\omega]+y_U[\omega]+\sigma^2} \leq \tau[\omega], \tag{46}$$

$$\mathbf{w}^H[\omega]E_\omega\mathbf{w}[\omega] = 1, \tag{47}$$

where the (e,f)-th element of $\mathbf{E}_\omega$, denoted by $[\mathbf{E}_\omega]_{e,f}$ is denoted by

$$[\mathbf{E}_\omega]_{e,f} = \begin{cases} 1 & e=f=n \\ 0 & \text{otherwise} \end{cases}. \tag{48}$$

Due to the fractional and non-concave constraint (46) in terms of $\mathbf{w}$, as well as the non-convex quadratic equality constraint (47) for each ω, finding the optimal solution for problem (44) is challenging. In order to address such issues, we employ the SDR approach in this case. Let $\text{rank}(Z)$ and $\text{tr}(Z)$ denote the rank and the trace of a matrix Z, respectively. With $\mathbf{W}[\omega] \triangleq \mathbf{w}[\omega]\mathbf{w}^H[\omega]$, the constraint of rank($\mathbf{W}[\omega]$) = 1 needs to be dropped in order to re-express problem (44) in its relaxed form. In order to obtain an approximate solution to problem (44), an updated optimization problem is shown below:

$$\max_{\mathbf{W}\succeq 0,\boldsymbol{\tau}\geq 0,\zeta} \ \zeta \tag{49}$$

$$\text{s.t.} \ \frac{1}{\Omega}\sum_{\omega=1}^{\Omega} \beta_i[\omega][\log_2(1+\text{tr}(\boldsymbol{\Phi}_W[\omega]\mathbf{W}[\omega])+y_W[\omega]) - \frac{\tau[\omega]}{\ln 2(1+\tau_0[\omega])}] \geq \zeta, \tag{50}$$

$$\frac{\text{tr}(\boldsymbol{\Phi}_I[\omega]\mathbf{W}[\omega])+y_I[\omega]}{\text{tr}(\boldsymbol{\Phi}_U[\omega]\mathbf{W}[\omega])+y_U[\omega]+\sigma^2} \leq \tau[\omega], \tag{51}$$

$$\text{tr}(\mathbf{E}_n\mathbf{W}[\omega]) = 1. \tag{52}$$

Using Charnes–Cooper transformation, setting $\varepsilon[\omega] = \frac{1}{[\text{tr}(\boldsymbol{\Phi}_U[\omega]\mathbf{W}[\omega])+y_U[\omega]+\sigma^2]}$ and $\mathbf{Y}[\omega] = \varepsilon[\omega]\mathbf{W}[\omega]$, and problem (49) can be further transformed to

$$\max_{\substack{\mathbf{W}\succeq 0,\varepsilon\succeq 0,\\ \mathbf{Y}\succeq 0,\boldsymbol{\tau}\geq 0,\zeta}} \ \zeta \tag{53}$$

$$\text{s.t.} \ \frac{1}{\Omega}\sum_{\omega=1}^{\Omega} \beta_i[\omega][\log_2(1+\frac{\text{tr}(\boldsymbol{\Phi}_W[\omega]\mathbf{Y}[\omega])}{\varepsilon[\omega]}+y_W[\omega]) - \frac{\tau[\omega]}{\ln 2(1+\tau_0[\omega])}] \geq \zeta, \tag{54}$$

$$\text{tr}(\boldsymbol{\Phi}_I[\omega]\mathbf{Y}[\omega]) + \varepsilon[\omega]y_I[\omega] \leq \tau[\omega], \tag{55}$$

$$\text{tr}(\mathbf{\Phi}_U[\omega]\mathbf{Y}[\omega]) + \varepsilon[\omega](y_U[\omega] + \sigma^2) = 1, \tag{56}$$
$$\text{tr}(\mathbf{E}_n\mathbf{Y}[\omega]) = \varepsilon[\omega], \tag{57}$$
$$(52).$$

With the assistance of the slack variable $\boldsymbol{\xi} = \xi[\omega]_{\omega=1}^{\Omega}$, problem (53) is transformed into an equivalent form that is non-fractional, shown as follows:

$$\max_{\substack{\mathbf{W}\succeq 0,\varepsilon\succeq 0,\\ \mathbf{Y}\succeq 0,\boldsymbol{\tau}\geq 0,\zeta}} \quad \zeta, \tag{58}$$
$$\text{s.t.} \quad \frac{1}{\Omega}\sum_{\omega=1}^{\Omega} \beta_i[\omega][\log_2(1+\xi[\omega]) - \frac{\tau[\omega]}{\ln 2(1+\tau_0[\omega])}] \geq \zeta \tag{59}$$
$$\xi[\omega] \leq \frac{\text{tr}(\mathbf{\Phi}_W[\omega]\mathbf{Y}[\omega])}{\varepsilon[\omega]} + y_W[\omega], \tag{60}$$
$$(52), (55)\text{–}(57).$$

Therefore, optimization problem (58) can be effectively addressed using CVX.

3.5. Optimization of the UAV Trajectory $\mathcal{T}$

Given $\mathbf{A}$, $\mathbf{P}_G$, $\mathbf{P}_U$ and $\mathbf{\Theta}$, the optimization problem of the UAV trajectory $\mathcal{T}$ can be expressed as

$$\max_{\mathcal{T},\zeta} \quad \zeta \tag{61}$$
$$\text{s.t.} \quad \frac{1}{\Omega}\sum_{\omega=1}^{\Omega} \beta_i[\omega][\log_2(1+\frac{P_G[\omega]}{\sigma^2 + P_U[\omega]\sigma_{RSI}^2}|\mathbf{h}_{G1}^H[\omega]\mathbf{H}_G u[\omega]|^2)$$
$$- \log_2(1+\frac{P_G[\omega]A[\omega]}{\sigma^2 + P_U[\omega]|\mathbf{h}_U^H[\omega]\mathbf{H}_U[\omega]u[\omega]|^2})] \geq \zeta, \tag{62}$$
$$(1), (2),$$

where

$$\mathbf{H}_G = \text{diag}\left(\begin{bmatrix} \mathbf{g}_{G,R} \\ 1 \end{bmatrix}\right), \mathbf{H}_U[\omega] = \text{diag}\left(\begin{bmatrix} \mathbf{g}_{U,R}[\omega] \\ 1 \end{bmatrix}\right),$$
$$\mathbf{h}_{G1}[\omega] = [\mathbf{g}_{R,U}^H[\omega], g_{G,U}[\omega]]^H, \mathbf{h}_{G2}[\omega] = [\mathbf{g}_{R,E}^H, g_{G,E}]^H, \mathbf{h}_U[\omega] = [\mathbf{g}_{R,E}^H, g_{U,E}[\omega]]^H,$$
$$A[\omega] = |\mathbf{h}_{G2}^H[\omega]\mathbf{H}_G u[\omega]|^2, \text{and } u[\omega] = [u_1[\omega], u_2[\omega], ..., u_N[\omega], 1]^T \left(u_n[\omega] = e^{j\theta_n[\omega]}, \forall\omega, n\right).$$

In particular, since $\mathbf{g}_{R,E}$ and $g_{G,E}$ are independent of the UAV trajectory, we set a constant $A[\omega]$ to replace it in (61). It is worth noting that $g_{G,U}[\omega]$, $g_{U,E}[\omega]$, and $\mathbf{g}_{R,U}[\omega]$ are impacted by the UAV trajectory from (3), (4), and (6). However, due to the complex and nonlinear nature of $\mathbf{g}_{R,U}[\omega]$ in (6), the optimization of the UAV trajectory becomes intractable. To address this issue, we approximate $\mathbf{g}_{R,U}[\omega]$ and $\mathbf{g}_{U,R}[\omega]$ in the j-th iteration using the UAV trajectory from the $(j-1)$-th iteration. With this approximation, we can reformulate problem (61) as follows:

$$\max_{\mathcal{T},\zeta} \quad \zeta, \tag{63}$$
$$\text{s.t.} \quad \frac{1}{\Omega}\sum_{\omega=1}^{\Omega} \beta_i[\omega][\log_2(1+\gamma_0[\omega]\mathbf{h}_{b,v}^T[\omega]\mathbf{H}_{i,Q}[\omega]\mathbf{h}_{b,v}[\omega])$$
$$- \log_2(1+\frac{\gamma_2[\omega]}{1+\gamma_1[\omega]\mathbf{h}_{c,v}^T[\omega]\mathbf{H}_{E,Q}[\omega]\mathbf{h}_{c,v}[\omega]})] \geq \zeta, \tag{64}$$
$$(1), (2),$$

where

$$\mathbf{h}_{b,v}[\omega] = \left[\sqrt{(dist_{G,U}[\omega])^{-\kappa_D}}, \sqrt{(dist_{U,R}[\omega])^{-\kappa_L}}\right]^T,$$

$$\mathbf{h}_{c,v}[\omega] = \left[\sqrt{(dist_{U,E}[\omega])^{-\kappa_D}}, \sqrt{(dist_{U,R}[\omega])^{-\kappa_L}}\right]^T,$$

$$\mathbf{H}_{i,Q}[\omega] = \left[\sqrt{\rho}\tilde{h}_1, \mathbf{g}_{G,R}^H \mathbf{\Theta}^H[\omega]\mathbf{g}_{R,U}^{\mathrm{LOS},(j-1)}[\omega]\right]^H \left[\sqrt{\rho}\tilde{h}_1, \mathbf{g}_{G,R}^H \mathbf{\Theta}^H[\omega]\mathbf{g}_{R,U}^{\mathrm{LOS},(j-1)}[\omega]\right],$$

$$\mathbf{H}_{E,Q}[\omega] = \left[\sqrt{\rho}\tilde{h}_2, (\mathbf{g}_{U,R}^{\mathrm{LOS},(j-1)}[\omega])^H \mathbf{\Theta}^H[\omega]\mathbf{g}_{R,E}\right]^H \left[\sqrt{\rho}\tilde{h}_2, (\mathbf{g}_{U,R}^{\mathrm{LOS},(j-1)}[\omega])^H \mathbf{\Theta}^H[\omega]\mathbf{g}_{R,E}\right].$$

Here, $\gamma_0[\omega] = \frac{P_G[\omega]}{\sigma^2 + P_U[\omega]\sigma_{RSI}^2}$, $\gamma_1[\omega] = \frac{P_U[\omega]}{\sigma^2}$, $\gamma_2[\omega] = \frac{P_G[\omega]A[\omega]}{\sigma^2}$, and $\mathbf{g}_{R,U}^{(j-1)}[\omega]$ and $\mathbf{g}_{U,R}^{(j-1)}[\omega]$ are the designed $\mathbf{g}_{U,R}[\omega]$ and $\mathbf{g}_{R,U}[\omega]$ utilizing the $(j-1)$-th iteration's UAV trajectory. Note that due to the objective function's non-concavity with regard to the UAV trajectory $\boldsymbol{\mathcal{T}}$, problem (63) is not convex. We further update problem (63) by introducing the slack variables $\mathbf{b} = b[\omega]_{\omega=1}^{\Omega}$, $\mathbf{v} = v[\omega]_{\omega=1}^{\Omega}$, $\mathbf{c} = c[\omega]_{\omega=1}^{\Omega}$, $\mathbf{f_0} = f_0[\omega]_{\omega=1}^{\Omega}$ and $\mathbf{f_1} = f_1[\omega]_{\omega=1}^{\Omega}$ into the optimization problem, shown as follows:

$$\max_{\substack{\boldsymbol{\mathcal{T}},\mathbf{b},\mathbf{v},\mathbf{c},\\ \mathbf{f}_0,\mathbf{f}_1,\zeta}} \quad \zeta, \tag{65}$$

$$\text{s.t.} \quad \frac{1}{\Omega}\sum_{\omega=1}^{\Omega} \beta_i[\omega][\log_2(1+\rho\gamma_0[\omega]f_0[\omega]) - \log_2(1+\frac{\gamma_2[\omega]}{1+\rho\gamma_1[\omega]f_1[\omega]})] \geq \zeta, \tag{66}$$

$$\sqrt{(dist_{G,U}[\omega])^{-\kappa_D}} \geq b[\omega], \tag{67}$$

$$\sqrt{(dist_{U,R}[\omega])^{-\kappa_L}} \geq v[\omega], \tag{68}$$

$$\sqrt{(dist_{U,E}[\omega])^{-\kappa_D}} \geq c[\omega], \tag{69}$$

$$\tilde{\mathbf{h}}_{b,v}^T[\omega]\mathbf{H}_{i,Q}[\omega]\tilde{\mathbf{h}}_{b,v}[\omega] \geq f_0[\omega], \tag{70}$$

$$\tilde{\mathbf{h}}_{c,v}^T[\omega]\mathbf{H}_{E,Q}[\omega]\tilde{\mathbf{h}}_{c,v}[\omega] \geq f_1[\omega], \tag{71}$$

$$(1), (2),$$

where $\tilde{\mathbf{h}}_{c,v}[\omega] = [c[\omega], v[\omega]]^T$ and $\tilde{\mathbf{h}}_{b,v}[\omega] = [b[\omega], v[\omega]]^T$. We unroll (67)–(69) in order to make the subsequent derivations easier, shown below:

$$x^2[\omega] + x_i^2 + y^2[\omega] + y_i^2 - 2x[\omega]x_i - 2y[\omega]y_i + z_U^2 - (b[\omega])^{-\frac{4}{\kappa_D}} \leq 0, \tag{72}$$

$$x^2[\omega] + x_R^2 + y^2[\omega] + y_R^2 - 2x[\omega]x_R - 2y[\omega]y_R + (z_U - z_R)^2 - (v[\omega])^{-\frac{4}{\kappa_L}} \leq 0, \tag{73}$$

$$x^2[\omega] + x_E^2 + y^2[\omega] + y_E^2 - 2x[\omega]x_E - 2y[\omega]y_E + z_U^2 - (c[\omega])^{-\frac{4}{\kappa_D}} \leq 0. \tag{74}$$

We utilize the SCA technique to handle the non-convexity of the constraints (72)–(74) and the non-concavity of $\log_2(1+\frac{\gamma_2[\omega]}{1+\rho\gamma_1[\omega]f_1[\omega]})$ respect to $f_1[\omega]$. And the first-order Taylor expansions of $(b[\omega])^{-\frac{4}{\kappa_D}}$, $(v[\omega])^{-\frac{4}{\kappa_L}}$, $(c[\omega])^{-\frac{4}{\kappa_D}}$, $\tilde{\mathbf{h}}_{b,v}^T[\omega]\mathbf{H}_{i,Q}[\omega]\tilde{\mathbf{h}}_{b,v}[\omega]$ and $\mathbf{h}_{c,v}^T[\omega]\mathbf{H}_{E,Q}[\omega]$ $\mathbf{h}_{c,v}[\omega]$ at the given feasible points $\mathbf{b}_0 = \{b_0[\omega]\}_{\omega=1}^{\Omega}$, $\mathbf{v}_0 = \{v_0[\omega]\}_{\omega=1}^{\Omega}$, $\mathbf{c}_0 = \{c_0[\omega]\}_{\omega=1}^{\Omega}$, $\mathbf{H}_{bv,0} = \{\tilde{\mathbf{h}}_{bv,0}[\omega]\}_{\omega=1}^{\Omega}$ and $\mathbf{H}_{cv,0} = \{\tilde{\mathbf{h}}_{cv,0}[\omega]\}_{\omega=1}^{\Omega}$ are given by

$$\tilde{\mathbf{h}}_{b,v}^T[\omega]\mathbf{H}_{i,Q}[\omega]\tilde{\mathbf{h}}_{b,v}[\omega] \geq -\tilde{\mathbf{h}}_{bv,0}^T[\omega]\mathbf{H}_{i,Q}[\omega]\tilde{\mathbf{h}}_{bv,0}[\omega] + 2\mathcal{R}\left[\tilde{\mathbf{h}}_{bv,0}^T[\omega]\mathbf{H}_{i,Q}[\omega]\tilde{\mathbf{h}}_{bv,0}[\omega]\right],$$

$$\tilde{\mathbf{h}}_{c,v}^T[\omega]\mathbf{H}_{E,Q}[\omega]\tilde{\mathbf{h}}_{c,v}[\omega] \geq -\tilde{\mathbf{h}}_{cv,0}^T[\omega]\mathbf{H}_{E,Q}[\omega]\tilde{\mathbf{h}}_{cv,0}[\omega] + 2\mathcal{R}\left[\tilde{\mathbf{h}}_{cv,0}^T[\omega]\mathbf{H}_{E,Q}[\omega]\tilde{\mathbf{h}}_{cv,0}[\omega]\right],$$

$$(b[\omega])^{-\frac{4}{\kappa_D}} \geq (b_0[\omega])^{-\frac{4}{\kappa_D}} - \frac{4}{\kappa_D}(b_0[\omega])^{-\frac{4}{\kappa_D}-1}(b[\omega] - b_0[\omega]),$$
$$(v[\omega])^{-\frac{4}{\kappa_L}} \geq (v_0[\omega])^{-\frac{4}{\kappa_L}} - \frac{4}{\kappa_L}(v_0[\omega])^{-\frac{4}{\kappa_L}-1}(v[\omega] - v_0[\omega]),$$
$$(c[\omega])^{-\frac{4}{\kappa_D}} \geq (c_0[\omega])^{-\frac{4}{\kappa_D}} - \frac{4}{\kappa_D}(c_0[\omega])^{-\frac{4}{\kappa_D}-1}(c[\omega] - c_0[\omega]).$$

Accordingly, problem (65) can be approximately transformed to

$$\max_{\substack{\mathcal{T},\mathbf{b},\mathbf{v},\mathbf{c},\\ \mathbf{f}_0,\mathbf{f}_1,\zeta}} \quad \zeta \tag{75}$$

$$\text{s.t.} \quad \frac{1}{\Omega}\sum_{\omega=1}^{\Omega} \beta_i[\omega][\log_2(1+\rho\gamma_0[\omega]f_0[\omega]) - \log_2(1+\frac{\gamma_2[\omega]}{1+\rho\gamma_1[\omega]f_1[\omega]})] \geq \zeta, \tag{76}$$

$$x^2[\omega] + x_i^2 + y^2[\omega] + y_i^2 - 2x[\omega]x_i - 2y[\omega]y_i + z_U^2 - (1+\frac{4}{\kappa_D})(b_0[\omega])^{-\frac{4}{\kappa_D}} + \frac{4}{\kappa_D}(b_0[\omega])^{-\frac{4}{\kappa_D}-1}b[\omega] \leq 0, \tag{77}$$

$$x^2[\omega] + x_R^2 + y^2[\omega] + y_R^2 - 2x[\omega]x_R - 2y[\omega]y_R + (z_U - z_R)^2 - (1+\frac{4}{\kappa_L})(v_0[\omega])^{-\frac{4}{\kappa_L}} + \frac{4}{\kappa_L}(v_0[\omega])^{-\frac{4}{\kappa_L}-1}v[\omega] \leq 0, \tag{78}$$

$$x^2[\omega] + x_E^2 + y^2[\omega] + y_E^2 - 2x[\omega]x_E - 2y[\omega]y_E + z_U^2 - (1+\frac{4}{\kappa_D})(c_0[\omega])^{-\frac{4}{\kappa_D}} + \frac{4}{\kappa_D}(c_0[\omega])^{-\frac{4}{\kappa_D}-1}c[\omega] \leq 0, \tag{79}$$

$$f_0[\omega] + \tilde{\mathbf{h}}_{bv,0}^T[\omega]\mathbf{H}_{i,Q}[\omega]\tilde{\mathbf{h}}_{bv,0}[\omega] - 2\mathcal{R}\left[\tilde{\mathbf{h}}_{bv,0}^T[\omega]\mathbf{H}_{i,Q}[\omega]\tilde{\mathbf{h}}_{bv,0}[\omega]\right] \leq 0, \tag{80}$$

$$f_1[\omega] + \tilde{\mathbf{h}}_{cv,0}^T[\omega]\mathbf{H}_{E,Q}[\omega]\tilde{\mathbf{h}}_{cv,0}[\omega] - 2\mathcal{R}\left[\tilde{\mathbf{h}}_{cv,0}^T[\omega]\mathbf{H}_{E,Q}[\omega]\tilde{\mathbf{h}}_{cv,0}[\omega]\right] \leq 0, \tag{81}$$

$$(1), (2).$$

Thus, the convex optimization problem (75) can be effectively addressed using CVX.

3.6. Algorithm Summary

Algorithm 1 provides a summary of the proposed algorithm, which decomposes the overall optimization problem into the five sub-problems. The maximum quantity of iterations is denoted by $l_{\max}$, and the convergence accuracy is controlled by parameter ϵ. As described in Section 2, by tackling the five subproblems iteratively, the solution to problem (21) can be obtained. The five subproblems' complexities determine the overall computational complexity. To solve these subproblems, the standard interior-point method is employed using CVX [34]. Subproblem 4 and subproblem 5 have the highest computational complexities, denoted as $O_{\text{sub4}}(\sqrt{N+1}\log(\frac{1}{\epsilon})(M\Omega(N+1)^3 + M^2\Omega^2(N+1)^2 + M^2\Omega^2))$ and $O_{\text{sub5}}((7N)^{3.5}\log(\frac{1}{\epsilon}))$, respectively. Therefore, the complexities of Algorithm 1 are mainly from subproblem 4 and subproblem 5. The objective function (21) in Algorithm 1 is confirmed by the subsequent numerical results.

4. Simulation Results

The proposed algorithm of jointly optimizing user scheduling, user transmit power, UAV jamming power, RIS phase shift and UAV trajectory, known as JO/SPPRT, can be verified in this section through some numerical simulation results. Unless otherwise specified, all parameters for simulations are shown in Table 2. The UAV initial feasible trajectory, called the baseline trajectory, follows a best-effort approach. It passes through the users along the direct path and proceeds directly to the destination point at its maximum speed within the UAV flying duration T. For the performance comparison, the following benchmarks are also considered in the simulation.

Algorithm 1 Overall algorithm for problem (21).

Initialize ${\mathbf{P_G}}^0$, ${\mathbf{P_U}}^0$, $\boldsymbol{\Theta}^0$, $\boldsymbol{\mathcal{T}}^0$, iteration number $l = 0$, tolerance ϵ and the maximum number of iterations $l_{\max}$.
repeat
  Set $l = l + 1$.
  Obtain $\boldsymbol{A}^l$ by solving problem (23) with given $\{{\mathbf{P_G}}^{l-1}, {\mathbf{P_U}}^{l-1}, \boldsymbol{\Theta}^{l-1}, \boldsymbol{\mathcal{T}}^{l-1}\}$.
  Obtain ${\boldsymbol{P_G}}^l$ by solving problem (26) with given $\{{\mathbf{P_U}}^{l-1}, \boldsymbol{\Theta}^{l-1}, \boldsymbol{\mathcal{T}}^{l-1}, \mathbf{A}^l\}$.
  Obtain ${\boldsymbol{P_U}}^l$ by solving problem (34) with given $\{\boldsymbol{\Theta}^{l-1}, \boldsymbol{\mathcal{T}}^{l-1}, \mathbf{A}^l, {\mathbf{P_G}}^l\}$.
  Obtain $\boldsymbol{\Theta}^l$ by solving problem (58) with given $\{\boldsymbol{\mathcal{T}}^{l-1}, \mathbf{A}^l, {\mathbf{P_G}}^l, {\mathbf{P_U}}^l\}$.
  Obtain $\boldsymbol{\mathcal{T}}^l$ by solving problem (75) with given $\{\mathbf{A}^l, {\mathbf{P_G}}^l, {\mathbf{P_U}}^l, \boldsymbol{\Theta}^l\}$.
  With given $\{\mathbf{A}^l, {\mathbf{P_G}}^l, {\mathbf{P_U}}^l, \boldsymbol{\Theta}^l$ and $\boldsymbol{\mathcal{T}}^l\}$, obtain ζ^l
until $|\zeta^l - \zeta^{l-1}| \le \epsilon$ or $l \ge l_{\max}$.

Table 2. Simulation parameters.

Notation	Physical Meaning	Simulation Parameters
$\mathbf{s}_G$	Horizontal location of ground users	$[-55, 15]^T$, $[0, 55]^T$, $[40, 20]^T$ m
$\mathbf{s}_E$	Horizontal location of the Eve	$[150, 70]^T$ m
$\mathbf{s}_R$	Horizontal location of the RIS	$[0, 0]^T$ m
z_R	RIS's placement height	80 m
$\mathbf{t}_0, \mathbf{t}_F$	UAV initial and final horizontal locations	$[-200, 40]^T$m, $[200, 40]^T$m
z_U	UAV flight altitude	100 m
$V_{\max}$	Maximum speed of UAV	30 m/s
δ_t	Each time slot's duration	1 s
$N = N_x \times N_z$	Quantity of RIS's reflecting elements	$N_x = 20, N_z = 10$
$\overline{P_G}, P_G^{\max}$	Ground user average and peak transmit power	0.1 W, 0.4 W
$\overline{P_U}, P_U^{\max}$	UAV average and peak jamming power	0.1 W, 0.4 W
$\kappa_D, \kappa_R, \kappa_L$	Corresponding path loss exponent	1.1, 2.2, 3.3
$\varrho_{G,R}, \varrho_{R,E}$	The Rician factor of the G-R, R-E link	3 dB
ρ	The path loss	−20 dB
σ^2	The additive white Gaussian noise power	−40 dBm
σ^2_{RSI}	The average loop interference level	−50 dBm

- JO/NJ: Joint optimization without jamming, which jointly optimizes the user scheduling, the user transmit power, the phase shift of RIS, and the trajectory of UAV by setting $P_U[\omega] = 0, \forall\omega$.
- JO/NR: Joint optimization without RIS, which jointly optimizes the user scheduling, the user transmit power, the UAV jamming power, and the UAV trajectory by setting the quantity of reflecting elements to be $N = 0, \forall\omega$.
- JO/NP: Joint optimization without power control, which jointly optimizes the user scheduling, the phase shift of RIS, and the trajectory of the UAV by setting the powers of the UAV and the users as $P_U[\omega] = \overline{P_U}$ and $P_G[\omega] = \overline{P_G}, \forall\omega$, respectively.

In Figure 2, the UAV trajectory is shown in terms of the four schemes when $T = 100$ s and $N = 200$. The specific descriptions for the optimal trajectories under four scenarios are shown as follows:

(1) In the proposed JO/SPPRT scheme, the UAV flies midway among the users and the RIS, maximizing the performance gain. Then, it approaches Eve, sending jamming signals to enhance communication security by suppressing eavesdropping.
(2) In the JO/NJ scheme, the UAV initially flies intermediately among the RIS and the users, maximizing the hovering time. Unlike the JO/SPPRT scheme, without jamming, the UAV focuses on flying away from the Eve to minimize eavesdropping.
(3) In the JO/NR scheme, the UAV communicates sequentially with user 2, user 1, and user 3. Different from the JO/SPPRT scheme, without the assistance of the RIS, the JO/NR scheme has limited ability to suppress eavesdropping. Hence, the UAV

approaches each user individually and moves away from the Eve to enhance the secrecy rate.

(4) In the JO/NP scheme, without power control, the users cannot transmit information at high power, and the UAV cannot send jamming signals at high power when close to Eve. Hence, the UAV flies midway among the RIS and the users to improve the communication performance, and moves away from the Eve to reduce eavesdropping.

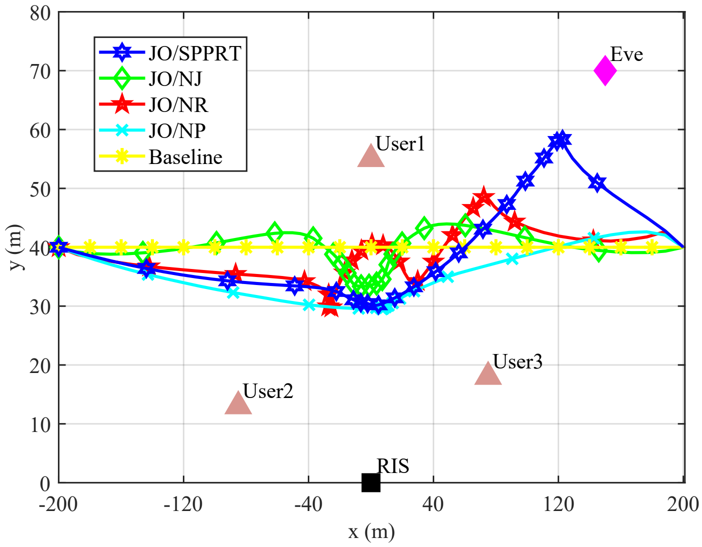

Figure 2. UAV trajectories with various benchmarks.

Figure 3 shows the max-min rate achieved under various schemes for varying T from 40 s to 160 s with $N = 200$. The JO/SPPRT scheme clearly outperforms other benchmarks. The JO/NJ scheme shows poor performance, as T increases because it cannot interfere with Eve. This shows the significant advantage of the UAV FD communication system. The JO/NP scheme outperforms the JO/NR scheme on the max-min rate, which shows that RIS can effectively suppress the eavesdropping. Obviously, the JO/SPPRT scheme outperforms the JO/NP scheme with respect to the secrecy rate, which demonstrates the effectiveness of the power optimization in boosting the overall secrecy rate.

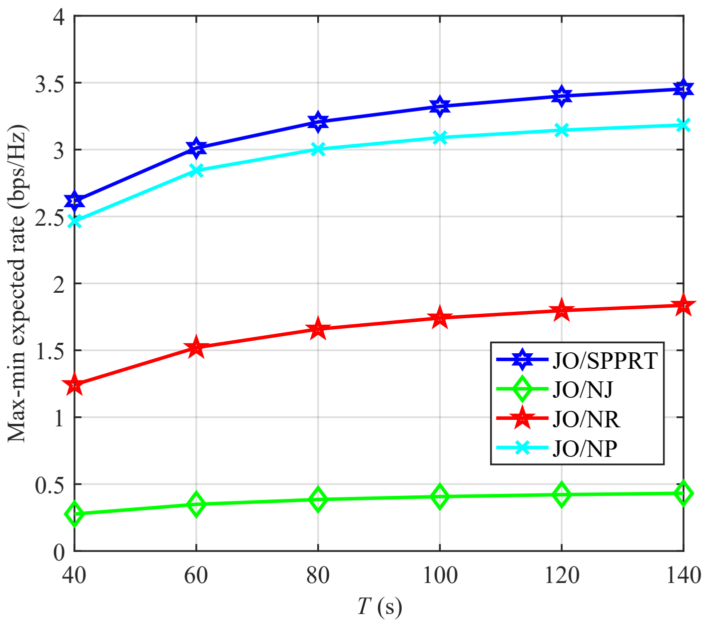

Figure 3. Max-min rate versus T with various benchmarks.

Figure 4 shows the achieved max-min rate with respect to T for $N = 200$, $N = 400$, and $N = 600$. For the same time slot, we can show that the higher the amount of the RIS reflecting elements N, the greater the secrecy rate improvement; for the same N value, the secrecy rate increases as T increases. Hence, increasing the number of elements can result in higher passive beamforming gain as observed in this figure.

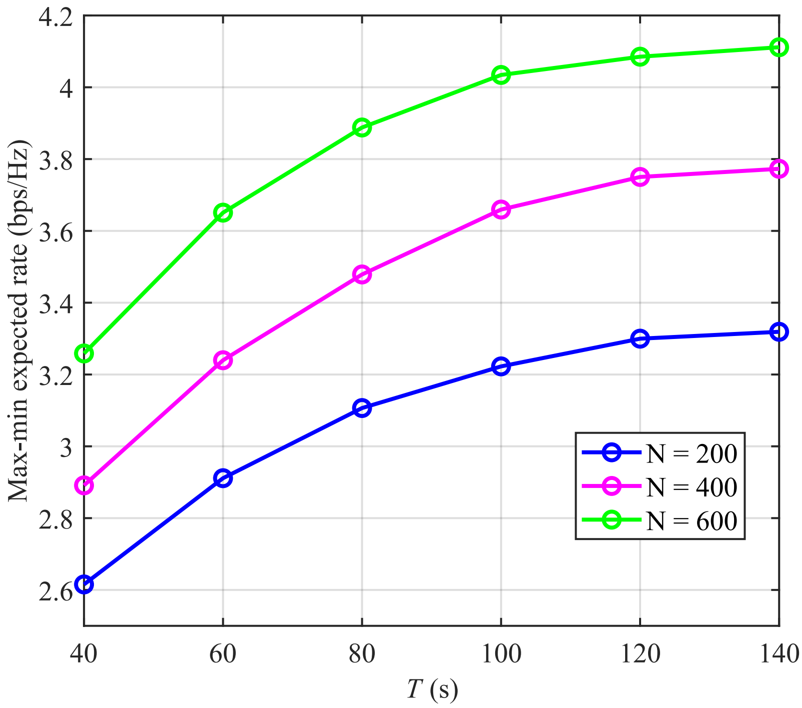

Figure 4. Max-min rate versus LIL (dBm) with various benchmarks.

Figure 5 shows the achieved max-min rate under different LIL for various benchmark schemes when $T = 100$ s and $N = 400$. The JO/SPPRT scheme demonstrates the superiority over other schemes. As LIL increases, the secrecy rate of JO/SPPRT approaches JO/NJ, while JO/NR converges to a stable value. In the JO/SPPRT scheme, the UAV dynamically adjusts the power allocation to align with the jamming power of the JO/NJ scheme, leading to the convergence of their secrecy rates, particularly in the scenarios with high LIL values. In the JO/NR scheme, the absence of RIS significantly reduces the communication performance and eavesdropping offset, and as LIL increases, it leads to a substantial decrease in the UAV jamming power and the convergence to a stable secrecy rate. Therefore, in the JO/SPPRT scheme, the higher LIL of the UAV will seriously affect its ability to send jamming signals. In the JO/NP scheme, with a fixed UAV jamming power, increasing the LIL of the UAV leads to intensified interference to the UAV airframe and a significant drop in the secrecy rate.

Figure 6 shows the jamming power with respect to T for various LIL when $N = 400$. In the JO/NR scheme, the jamming power shows three phases as follows. Firstly, during communication between the UAV and user 2, the jamming power requirement is minimal, as user 2 is farthest from Eve. Secondly, as the UAV communicates with user 3, since user 3 is closer to Eve, the jamming power needs to be set to a higher value. Lastly, the higher jamming power is required to counteract eavesdropping when the UAV communicates with user 1, which is closest to the Eve. We can see that the higher LIL results in the lower jamming power at each stage, and excessive LIL significantly hampers the effectiveness of UAV in jamming the Eve. Also, we can observe that the JO/SPPRT scheme maintains a low and steady jamming power throughout the stage, which is less affected by LIL. As such, we can show that compared to the JO/NR scheme, the JO/SPPRT scheme with the aid of RIS provides the best security performance with less jamming power. This also shows the fact that the JO/SPPRT scheme with RIS reduces the communication energy usage and reduces the effect of RSI on the secure communication of FD UAV.

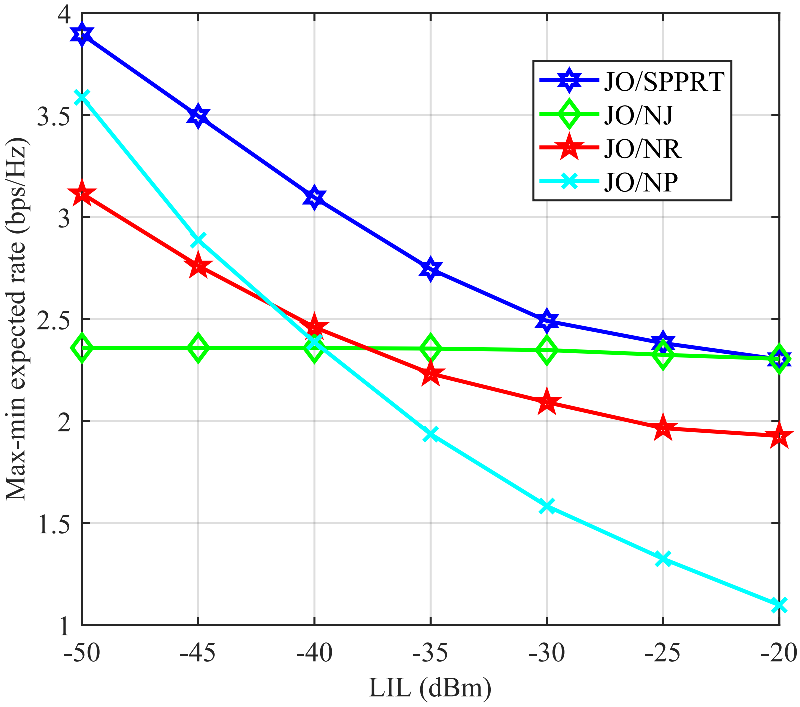

Figure 5. Max-min rate versus LIL (dBm) with various benchmarks.

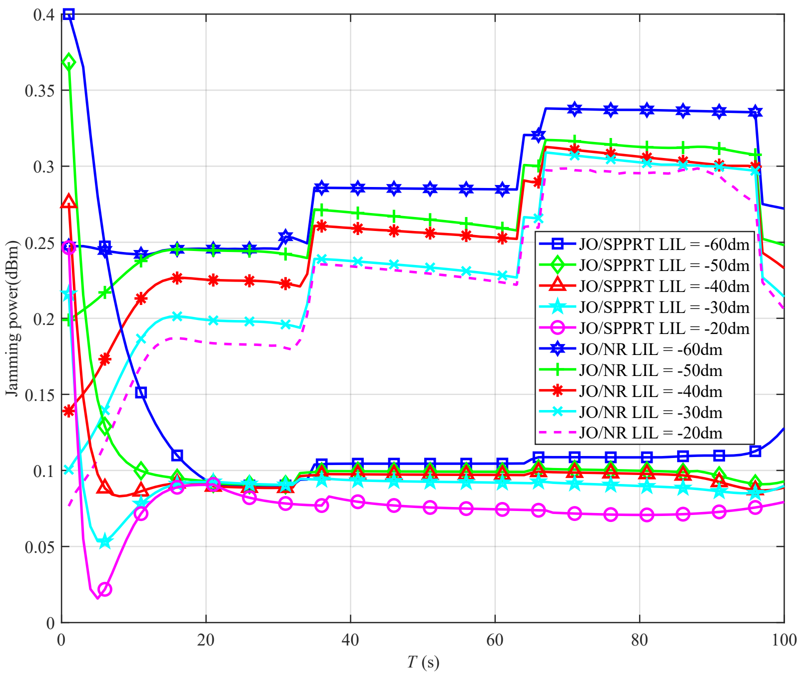

Figure 6. Jamming power of UAV versus LIL (dBm).

5. Conclusions

In this paper, we investigated an RIS-assisted FD UAV secure communication system. We maximized the worst-case average secrecy rate by jointly optimizing several parameters, such as user scheduling, user transmit power, UAV jamming power, RIS phase shift, and UAV trajectory. Due to the non-convexity of the optimization problem and the presence of non-convex quadratic equality constraints in the subproblems, we proposed a novel algorithm, namely the JO/SPPRT scheme, to handle such an optimization problem and obtain a suboptimal solution. The numerical results confirmed the effectiveness of our proposed algorithm. Furthermore, we obtained the following conclusions: (1) The RIS-assisted FD UAV under RSI has the higher capability to interfere with eavesdropping, and results in further security enhancement as well as reducing the effect of RSI on FD UAV communication. (2) Unlike work that solely considered LoS channels, our research considered Rayleigh channels for direct links and Rician and LoS channels for reflected links, which can better match the actual environment condition in urban areas. Accordingly, this approach further enhances security performance and reduces biases and losses. (3) As compared to the scheme without RIS, our proposed scheme showed better security performance with lower jamming power. As such, our scheme is more energy saving.

Although this study addresses a scenario involving single eavesdropper, the proposed algorithm can be extended to the general case of multiple eavesdroppers. Additionally, this work could be further advanced using state-of-the-art reinforcement learning techniques for optimization. The algorithm proposed in this paper can serve as a benchmark to assess the performance and efficacy of such reinforcement learning algorithms.

Author Contributions: Conceptualization, methodology, and software, H.L. and B.D.; Validation, H.L.; Investigation, D.L., J.N., X.W. and Y.H.; Writing—original draft preparation H.L.; Writing—review and editing, B.D. and F.X. All authors have read and agreed to the published version of the manuscript.

Funding: This work was supported by the National Natural Science Foundation of China (62172060), and the Sichuan Science and Technology Program under Grant (No.2023YFH0092, No.2022YFQ0017).

Institutional Review Board Statement: Not applicable.

Informed Consent Statement: Not applicable.

Data Availability Statement: The code is available on request.

Conflicts of Interest: The authors declare no conflict of interest.

References

1. Shakhatreh, H.; Sawalmeh, A.H.; Al-Fuqaha, A.; Dou, Z.; Almaita, E.; Khalil, I.; Othman, N.S.; Khreishah, A.; Guizani, M. Unmanned Aerial Vehicles (UAVs): A Survey on Civil Applications and Key Research Challenges. *IEEE Access* **2019**, *7*, 48572–48634. [CrossRef]
2. Menouar, H.; Guvenc, I.; Akkaya, K.; Uluagac, A.S.; Kadri, A.; Tuncer, A. UAV-Enabled Intelligent Transportation Systems for the Smart City: Applications and Challenges. *IEEE Commun. Mag.* **2017**, *55*, 22–28. [CrossRef]
3. Kim, J.; Kim, S.; Ju, C.; Son, H.I. Unmanned Aerial Vehicles in Agriculture: A Review of Perspective of Platform, Control, and Applications. *IEEE Access* **2019**, *7*, 105100–105115. [CrossRef]
4. Akyildiz, I.F.; Kak, A.; Nie, S. 6G and Beyond: The Future of Wireless Communications Systems. *IEEE Access* **2020**, *8*, 133995–134030. [CrossRef]
5. Mozaffari, M.; Saad, W.; Bennis, M.; Nam, Y.H.; Debbah, M. A Tutorial on UAVs for Wireless Networks: Applications, Challenges, and Open Problems. *IEEE Commun. Surv. Tutor.* **2019**, *21*, 2334–2360. [CrossRef]
6. Li, B.; Fei, Z.; Zhang, Y. UAV Communications for 5G and Beyond: Recent Advances and Future Trends. *IEEE Internet Things J.* **2019**, *6*, 2241–2263. [CrossRef]
7. Cui, M.; Zhang, G.; Wu, Q.; Ng, D.W.K. Robust Trajectory and Transmit Power Design for Secure UAV Communications. *IEEE Trans. Veh. Technol.* **2018**, *67*, 9042–9046. [CrossRef]
8. Wang, D.; Bai, B.; Zhao, W.; Han, Z. A Survey of Optimization Approaches for Wireless Physical Layer Security. *IEEE Commun. Surv. Tutor.* **2019**, *21*, 1878–1911. [CrossRef]
9. Deng, H.; Wang, H.M.; Guo, W.; Wang, W. Secrecy Transmission with a Helper: To Relay or to Jam. *IEEE Trans. Inf. Forensics Secur.* **2015**, *10*, 293–307. [CrossRef]
10. Li, A.; Wu, Q.; Zhang, R. UAV-Enabled Cooperative Jamming for Improving Secrecy of Ground Wiretap Channel. *IEEE Wirel. Commun. Lett.* **2019**, *8*, 181–184. [CrossRef]
11. Mamaghani, M.T.; Hong, Y. Joint Trajectory and Power Allocation Design for Secure Artificial Noise Aided UAV Communications. *IEEE Trans. Veh. Technol.* **2021**, *70*, 2850–2855. [CrossRef]
12. Zhong, C.; Yao, J.; Xu, J. Secure UAV Communication with Cooperative Jamming and Trajectory Control. *IEEE Commun. Lett.* **2019**, *23*, 286–289. [CrossRef]

13. Tang, J.; Chen, G.; Coon, J.P. Secrecy Performance Analysis of Wireless Communications in the Presence of UAV Jammer and Randomly Located UAV Eavesdroppers. *IEEE Trans. Inf. Forensics Secur.* **2019**, *14*, 3026–3041. [CrossRef]
14. Cheng, T.; Wang, B.; Cao, K.; Dong, R.; Diao, D. IRS-Enabled Secure G2A Communications for UAV System with Aerial Eavesdropping. *IEEE Syst. J.* **2022**, *17*, 3670–3681. [CrossRef]
15. Amri, M.M.; Tran, N.M.; Park, J.H.; Kim, D.I.; Choi, K.W. Demo: Demonstration of reconfigurable intelligent surface (RIS)-assisted simultaneous wireless information and power transfer (SWIPT). In Proceedings of the 2022 IEEE International Conference on Communications Workshops (ICC Workshops), Seoul, Republic of Korea, 16–20 May 2022; pp. 1–2. [CrossRef]
16. Liu, Y.; Liu, X.; Mu, X.; Hou, T.; Xu, J.; Di Renzo, M.; Al-Dhahir, N. Reconfigurable Intelligent Surfaces: Principles and Opportunities. *IEEE Commun. Surv. Tutor.* **2021**, *23*, 1546–1577. [CrossRef]
17. Liaskos, C.; Nie, S.; Tsioliaridou, A.; Pitsillides, A.; Ioannidis, S.; Akyildiz, I. A New Wireless Communication Paradigm through Software-Controlled Metasurfaces. *IEEE Commun. Mag.* **2018**, *56*, 162–169. [CrossRef]
18. Shen, A.; Luo, J.; Ning, J.; Li, Y.; Wang, Z.; Duo, B. Safeguarding UAV Networks against Active Eavesdropping: An Elevation Angle-Distance Trade-Off for Secrecy Enhancement. *Drones* **2023**, *7*, 109. [CrossRef]
19. Wu, Q.; Zhang, R. Towards Smart and Reconfigurable Environment: Intelligent Reflecting Surface Aided Wireless Network. *IEEE Commun. Mag.* **2020**, *58*, 106–112. [CrossRef]
20. Wu, Q.; Zhang, S.; Zheng, B.; You, C.; Zhang, R. Intelligent Reflecting Surface-Aided Wireless Communications: A Tutorial. *IEEE Trans. Commun.* **2021**, *69*, 3313–3351. [CrossRef]
21. Fang, S.; Chen, G.; Li, Y. Joint Optimization for Secure Intelligent Reflecting Surface Assisted UAV Networks. *IEEE Wirel. Commun. Lett.* **2021**, *10*, 276–280. [CrossRef]
22. Ye, Z.; Su, G.; Chen, B.; Dai, M.; Lin, X.; Wang, H. Secrecy rate optimization for secure communication in IRS-Aided UAV systems. In Proceedings of the 2022 31st Wireless and Optical Communications Conference (WOCC), Shenzhen, China, 20–24 May 2022; pp. 6–11. [CrossRef]
23. Pang, X.; Zhao, N.; Tang, J.; Niyato, D.; Wong, K.K. Joint trajectory and beamforming optimization for secure UAV transmission aded by IRS. In Proceedings of the 2021 13th International Conference on Wireless Communications and Signal Processing (WCSP), Virtual Conference, 20–22 October 2021; pp. 1–6. [CrossRef]
24. Wang, H.M.; Zhang, X.; Jiang, J.C. UAV-Involved Wireless Physical-Layer Secure Communications: Overview and Research Directions. *IEEE Wirel. Commun.* **2019**, *26*, 32–39. [CrossRef]
25. Li, Z.; Chen, W.; Wu, Q.; Wang, K.; Li, J. Joint Beamforming Design and Power Splitting Optimization in IRS-Assisted SWIPT NOMA Networks. *IEEE Trans. Wirel. Commun.* **2022**, *21*, 2019–2033. [CrossRef]
26. Duo, B.; Wu, Q.; Yuan, X.; Zhang, R. Energy Efficiency Maximization for Full-Duplex UAV Secrecy Communication. *IEEE Trans. Veh. Technol.* **2020**, *69*, 4590–4595. [CrossRef]
27. Liu, G.; Yu, F.R.; Ji, H.; Leung, V.C.M.; Li, X. In-Band Full-Duplex Relaying: A Survey, Research Issues and Challenges. *IEEE Commun. Surv. Tutor.* **2015**, *17*, 500–524. [CrossRef]
28. Nguyen, T.T.; Hoang, V.T.; Le, T.T.H.; Tran, X.N. Physical layer security for UAV-based full-duplex relay NOMA system. In Proceedings of the 2022 International Conference on Advanced Technologies for Communications (ATC), Hanoi, Vietnam, 20–22 October 2022; pp. 395–400. [CrossRef]
29. Tian, K.; Duo, B.; Li, S.; Zuo, Y.; Yuan, X. Hybrid Uplink and Downlink Transmissions for Full-Duplex UAV Communication with RIS. *IEEE Wirel. Commun. Lett.* **2022**, *11*, 866–870. [CrossRef]
30. Lin, X.; Yajnanarayana, V.; Muruganathan, S.D.; Gao, S.; Asplund, H.; Maattanen, H.L.; Bergstrom, M.; Euler, S.; Wang, Y.P.E. The Sky Is Not the Limit: LTE for Unmanned Aerial Vehicles. *IEEE Commun. Mag.* **2018**, *56*, 204–210. [CrossRef]
31. Wei, Z.; Cai, Y.; Sun, Z.; Ng, D.W.K.; Yuan, J.; Zhou, M.; Sun, L. Sum-Rate Maximization for IRS-Assisted UAV OFDMA Communication Systems. *IEEE Trans. Wirel. Commun.* **2021**, *20*, 2530–2550. [CrossRef]
32. Gopala, P.K.; Lai, L.; El Gamal, H. On the Secrecy Capacity of Fading Channels. *IEEE Trans. Inf. Theory* **2008**, *54*, 4687–4698. [CrossRef]
33. Li, S.; Duo, B.; Renzo, M.D.; Tao, M.; Yuan, X. Robust Secure UAV Communications with the Aid of Reconfigurable Intelligent Surfaces. *IEEE Trans. Wirel. Commun.* **2021**, *20*, 6402–6417. https://doi.org/10.1109/TWC.2021.3073746.
34. Grant, S.B.M. CVX: Matlab Software for Disciplined Convex Programming, Version 2.2. 2020. Available online: http://cvxr.com/cvx (accessed on 20 September 2021).